American Mineralogist, Volume 63, pages 1198–1208, 1978

Lattice dynamics of forsterite

KAZUAKI IISHI[1]

Mineralogisches Institut der Technischen Universität Hannover
3000 Hannover, West Germany

Abstract

Detailed experimental and theoretical studies of the $\mathbf{k} = \mathbf{0}$ vibrational spectra of the orthorhombic crystal forsterite (Mg_2SiO_4) are reported. The polarized infrared reflection spectra and the Raman spectra of a single crystal were measured. The short-range force constants and the contribution of potential terms to the elastic constants were calculated from explicit expressions for elastic constants and for optical frequencies. The elastic constant of forsterite is attributable mainly to the Mg–O stretching force and the O···O repulsive force among SiO_4 tetrahedra. The frequencies of the phonon spectrum and the contribution of potential terms to potential energy were also calculated, based both on a rigid-ion model and on a polarizable-ion model. The rigid-ion model explains well the magnitudes of the experimental *TO–LO* frequency splitting. The best set of effective charge is found to be $Z_{Mg} = 0.93$, $Z_{Si} = 0.70$, and $Z_O = -0.64e$. New assignments are deduced from theoretical vibrational modes and are discussed with results of previous work. The electronic polarizability is found to be $\alpha(Mg) = 0.1$, $\alpha(Si) = 0.05$, $\alpha_{xx}(O) = 1.55$, $\alpha_{yy}(O) = 1.50$ and $\alpha_{zz}(O) = 1.55 A^3$. In spite of the more elaborate nature of the polarizable-ion model, the agreement for the optical frequencies is not improved as compared with the rigid-ion model.

Introduction

In spite of the interest and importance of forsterite lattice dynamics for mineralogists and geophysicists, few studies on this problem have been carried out. This lack is most probably related to the orthorhombic symmetry and complexity of the crystal structure, which make a detailed and unique interpretation of the spectrum difficult.

Tarte (1963) studied powder infrared absorption measurements by isomorphic substitution, and interpreted observed spectra by the use of the vibration of SiO_4 tetrahedra and XO_6 octahedra, where X = Mg,Ca,Ni,Co,Fe,Mn. Duke and Stephens (1964) studied influences of divalent cations on vibrational frequencies of the SiO_4 tetrahedron. Paques-Ledent and Tarte (1973) investigated the infrared and Raman spectra of the isotopic species of the type compound Mg_2SiO_4, and deduced new assignments from ^{24}Mg–^{26}Mg and ^{28}Si–^{30}Si isotopic shifts. They made their assignments more definitive by investigating the infrared and Raman spectra of olivine-type orthophosphates, -arsenates and -vanadates $A^IB^{II}X^VO_4$ (1974) and those of olivine-type orthosilicates and germanates $A^IB^{III}X^{IV}O_4$ (Paques-Ledent, 1976).

Servoin and Piriou (1973) studied infrared reflectivity and Raman scattering spectra of a synthetic forsterite crystal. They found most of the infrared lattice bands by the analysis of reflectivity data based on a classical dispersion theory and found all the modes predicted in the Raman spectra. Ochler and Günthard (1969) determined a set of force constants from data on powder infrared spectra, by means of normal coordinate calculation in the center of the Brillouin zone.

This paper includes data on the infrared reflectivity and Raman scattering spectra of a synthetic forsterite single crystal and the calculation of lattice dynamics in the center of the Brillouin zone. Also presented are: (1) information about the nature of short-range and Coulomb interactions and the microscopic nature of elastic constants; and (2) more comprehensive interpretation of the spectra on combined use of theoretical vibrational modes and existing spectrum data on pure compounds, solid solutions, and isotopic species.

Group theory analysis

Forsterite is an ionic crystal belonging to the orthorhombic space group *Pbnm*, $Z = 4$. The irreduc-

[1] On leave from the Department of Mineralogical Sciences, Faculty of Literature and Science, Yamaguchi University, Yamaguchi, 753 Japan (present address), with support from the Alexander von Humboldt Foundation.

0003-004X/78/1112-1198$02.00

ible representation corresponding to the forsterite lattice is:

$$\Gamma_t = 11A_g + 7B_{1g} + 11B_{2g} + 7B_{3g} + 10A_u + 14B_{1u} + 10B_{2u} + 14B_{3u}$$

A detailed group theoretical analysis was reported by Paques-Ledent and Tarte (1973).

The free SiO_4 ion, of point group T_d, has four different modes of vibration: $\nu_1(A_1$ type), ν_2 (E type), ν_3 and ν_4 (F_2 type). In the forsterite lattice, however, each SiO_4 ion occupies site of C_s symmetry, and the anisotropic crystal field results in complete lifting of degeneracies of the SiO_4 "internal" modes: $4\nu_1(A_1) \rightarrow A_g + B_{2g} + B_{1u} + B_{3u}$; $4\nu_2(E) \rightarrow A_g + B_{1g} + B_{2g} + B_{3g} + A_u + B_{1u} + B_{2u} + B_{3u}$; and $4\nu_3(F_2)$ and $4\nu_4(F_2) \rightarrow 2A_g + B_{1g} + 2B_{2g} + B_{3g} + A_u + 2B_{1u} + B_{2u} + 2B_{3u}$ ($\times 2$). The external modes are separated into rotatory types of SiO_4 ion and translatory types of SiO_4 and Mg ion. Magnesium ions at MgI site (C_i symmetry) do not change during the Raman active vibration.

Experimental results and discussion

Raman spectra

The single-crystal boule used was grown by Takei and Kobayashi (1974) by the Czochralski method. The properties of the single crystal reported by them are: (1) optically uniform; (2) free from visible inhomogeneities such as bubbles, inclusions, and cracks; (3) nonstoichiometric excess of Mg ions of 0.7 to 2.4 mole percent; (4) impurity of several hundred weight ppm of Fe; and (5) contamination of about 17 weight ppm of iridium. This single crystal seems good to measure the infrared and Raman spectra. All measurements were carried out on three samples cut from the original boule. The samples were oriented by the use of X-rays. The selected three faces (100), (010), and (001) were ground and polished using carborundum and diamond paste. Average sample dimension was $10 \times 5 \times 5$ mm.

The Raman spectra were recorded with a Czerny-Turner spectrometer and a 3-Watt-Spectra-Physics argon ion laser at 4880A. The experimental arrangement was described by Salje (1974).

Four Raman spectra of forsterite are shown in Figure 1, and the Raman line frequencies are listed in Table 1. Results are the same as a previous investigation (Servoin and Piriou, 1973) except the following: (1) a weak line at 224cm^{-1} instead of their 164cm^{-1} in B_{1g} symmetry; (2) a weak but clear line at 142cm^{-1} in place of their 407cm^{-1} in B_{2g} symmetry; (3) two weak lines at 272 and 226cm^{-1} different from their 484 and 466cm^{-1} in B_{3g} symmetry.

Infrared spectra

Infrared reflection spectra were recorded under normal incidence using a Beckman instrument in the frequency range 250 to 1200cm^{-1}. Polarized infrared

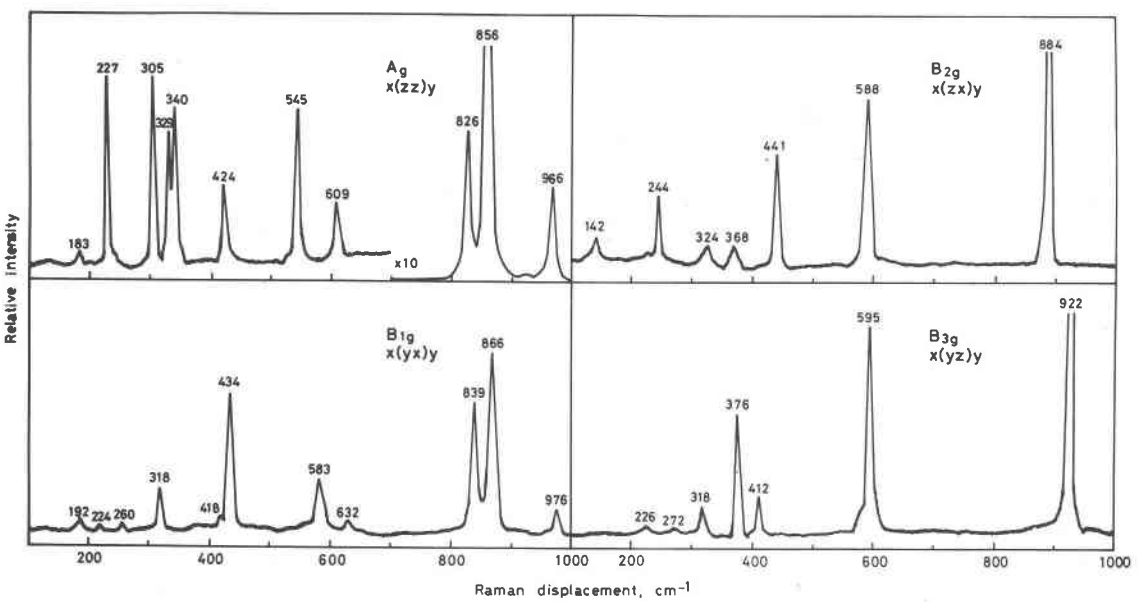

Fig. 1. Polarized Raman spectra of forsterite.

radiation was obtained by the use of a wire grid type polarizer of AgCl. The same samples used in the Raman spectra measurements were employed. The spectra were analysed by classical dispersion theory (Salje and Iishi, 1977). The classical oscillator parameter values of transverse optical frequency ν_{TO}, oscillator strength $\Delta\epsilon$ and damping constant γ were determined, so that the calculated reflectivity coincides with the experimental ones. The calculated curve with the parameters listed in Table 2 agreed well with the experimental reflection spectra.

A comparison with a previous measurement of Servoin and Piriou (1973) reveals reasonable agreement, except the frequencies at 365cm^{-1} of B_{1u} and 562cm^{-1} of B_{3u}. These two peaks are weak but are found in the present reflectivity measurements of B_{1u} and B_{3u} mode spectra. Owing to the limit in the available spectral range of our apparatus, we cannot find all modes expected from factor group analysis (Servoin and Piriou, 1973). In the present lattice dynamical calculation, we used probable assignment of vibrational frequencies of powder in the low frequency region under 250cm^{-1} of Ochler and Günthard (1969).

Paques-Ledent and Tarte (1973, 1974) and Paques-Ledent (1976) interpreted the infrared spectra of olivine by the combined use of isotropic studies and group theoretical considerations, together with a previous assignment by Tarte (1963) by the isomorphic substitution method. In the present lattice dynamical calculations, their assignments are used to determine dynamical parameters.

The frequency values of infrared active mode listed in Table 2 were used for the lattice dynamical calculation, together with those of Raman active mode in Table 1. The mode assignment problem will be discussed by the use of the information of the theoretical vibrational modes derived from the lattice dynamical calculation.

Method of calculation

The projection of the structure of forsterite on the (001) and (100) planes in Figure 2 shows the atomic positions used in this paper. Unit-cell dimensions and

Table 1. Experimental and theoretical frequencies (cm^{-1}) and assignments of forsterite (Raman spectra)

Sym.	Mode	Exp.	Theoretical SR1	RI3	PI3	Assignments*	Sym.	Mode	Exp.	Theoretical SR1	RI3	PI3	Assignments*
A_g	ν_{11}	966	968	958	962	ν_3	B_{1g}	ν_{21}	976	966	961	962	ν_3
	ν_{12}	856	888	888	886	ν_3		ν_{22}	866	888	891	888	ν_3
	ν_{13}	826	840	837	839	ν_1		ν_{23}	839	839	846	839	ν_1
	ν_{14}	609	600	606	598	ν_4		ν_{24}	632	614	629	616	ν_4
	ν_{15}	546	542	535	537	ν_4		ν_{25}	583	518	583	519	ν_4
	ν_{16}	424	441	414	430	ν_2		ν_{26}	434	420	412	418	ν_2
	ν_{17}	340	357	358	350	R'(SiO_4:z)		ν_{27}	418	405	396	394	R'(SiO_4:z)
	ν_{18}	329	321	287	318	T'(MgII:y)		ν_{28}	318	319	316	333	T'(MgII:y)
	ν_{19}	305	256	269	269	T'(MgII,SiO_4:x)		ν_{29}	260	269	276	287	T'(MgII,SiO_4:x)
	ν_{110}	227	206	228	213	T'(SiO_4,MgII:y)		ν_{210}	224	215	230	217	T'(MgII,SiO_4:x)
	ν_{111}	183	169	157	165	T'(MgII,SiO_4:x)		ν_{211}	192	207	180	206	T'(SiO_4,MgII:y)
B_{2g}	ν_{31}	884	894	891	894	ν_3	B_{3g}	ν_{41}	922	893	894	894	ν_3
	ν_{32}	588	558	591	563	ν_4		ν_{42}	595	543	580	548	ν_4
	ν_{33}	441	476	451	467	ν_2		ν_{43}	412	424	411	424	ν_2
	ν_{34}	368	373	362	373	R'(SiO_4:y)		ν_{44}	376	361	c67	362	R'(SiO_4:z)
	ν_{35}	324	307	306	312	R'(SiO_4:x)		ν_{45}	318	325	304	323	R'(SiO_4:y)
	ν_{36}	244	264	267	268	T'(SiO_4:z)		ν_{46}	272	270	277	269	T'(MgII:z)
	ν_{37}	142	159	166	157	T'(MgII:z)		ν_{47}	226	234	234	242	T'(SiO_4:z)

* *R': rotational lattice mode, T': translational lattice mode.*

Table 2. Experimental and theoretical frequencies (cm^{-1}) and assignments of forsterite (infrared spectra)

Sym.	Mode	Experimental				Theoretical					Assignments*
						SR1	RI3		PI3		
		ν_{TO}	ν_{LO}	$\Delta\varepsilon$	γ	ν_{TO}	ν_{TO}	ν_{LO}	ν_{TO}	ν_{LO}	
B_{1u}	ν_{61}	885	994	0.54	6.4	894	890	913	893	903	ν_3
	ν_{62}	502	585	0.39	6.8	527	492	540	512	512	ν_4
	ν_{63}	483	489	0.25	15.8	473	480	491	482	494	ν_2
	ν_{64}	423	459	1.24	8.1	443	417	420	439	444	R'(SiO_4:y)
	ν_{65}	365	371	0.28	33.0	391	345	362	391	391	R'(SiO_4:z)
	ν_{66}	296	318	1.29	6.2	336	309	343	336	350	T'(MgI:z)
	ν_{67}	274	278	0.20	7.6	251	266	274	240	244	T'(MgI:y; MgII:z)
	ν_{68}	224[b]				214	230	231	209	209	T'(MgI:x)
	ν_{69}	201[b]				183	208	209	185	186	T'(MgI:y,z)
B_{2u}	ν_{71}	987	993	0.002	8.0	964	957	958	958	959	ν_3
	ν_{72}	882	979	0.43	10.8	894	897	917	900	906	ν_3
	ν_{73}	838	843	0.08	12.0	837	833	833	834	834	ν_1
	ν_{74}	537	597	0.36	9.5	582	581	584	581	581	ν_4
	ν_{75}	510	516	0.04	8.0	554	543	560	542	543	ν_4
	ν_{76}	465	493	0.27	10.4	460	467	513	467	479	ν_2
	ν_{77}	421	446	0.38	6.8	433	417	423	427	430	R'(SiO_4:z)
	ν_{78}	400	412	0.45	9.1	353	357	359	364	364	T'(MgI:z)
	ν_{79}	352	376	1.23	9.5	336	321	344	338	354	T'(MgII:x,y)
	ν_{710}	294	313	1.47	6.8	274	314	312	284	284	T'(MgIx,z; MgII:y)
	ν_{711}	280	283	0.19	6.2	246	278	297	250	250	T'(MgI:y)
	ν_{712}	224[b]				216	235	238	224	225	T'(MgII:x)
	ν_{713}	144[b]				135	139	140	137	138	T'(MgI,SiO_4:x)
B_{3u}	ν_{81}	980	1086	0.38	15.8	964	956	976	957	967	ν_3
	ν_{82}	957	963	0.12	11.4	893	915	916	901	901	ν_3
	ν_{83}	838	845	0.02	22.0	836	826	827	832	835	ν_1
	ν_{84}	601	645	0.21	13.0	574	565	601	569	577	ν_4
	ν_{85}	562	566	0.02	13.9	543	527	527	529	528	ν_4
	ν_{86}	498	544	0.35	18.8	459	493	494	473	473	ν_2
	ν_{87}	403	469	1.27	6.2	427	403	413	421	421	R'(SiO_4:x)
	ν_{88}	378	386	1.59	18.0	353	362	392	359	376	T'(MgI:z)
	ν_{89}	320	323	0.17	7.4	322	312	347	327	332	T'(MgI:z,y)
	ν_{810}	293	298	0.40	6.3	271	303	309	280	280	T'(MgI:x,z)
	ν_{811}	274	276	0.08	4.2	239	264	265	242	241	T'MgI:x; MgII:y)
	ν_{812}	224[b]				216	238	242	218	219	T'(MgII:x,y)
	ν_{813}	201[b]				186	188	190	190	191	T'(MgI,SiO_4:y)

* *R': rotational lattice mode, T': translational lattice mode.* *b) Probable assignment from powder data of Ochler and Günthard (1969).*

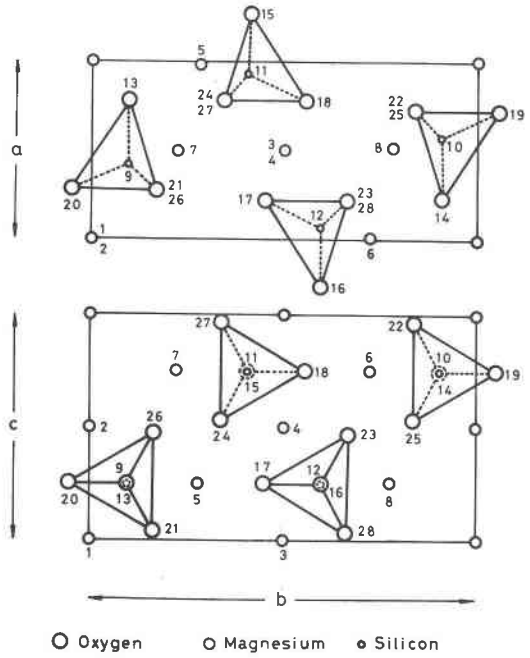

Fig. 2. Labelling of atoms in the crystal structure of forsterite, *Pbnm*. Unit cell dimensions are a = 4.762, b = 10.225 and c = 5.994A.

the atomic parameters are taken from Birle *et al.* (1968). A group theoretical analysis was carried out on the symmetry properties of the normal modes of vibration following the method described by Chen (1967). There is good agreement between several different measurements of the elastic constant. Values obtained by Graham and Barsch (1969) were used.

The elastic constant was calculated by the method of Shiro and Miyazawa (1971). The contribution of the potential term to the elastic constant $(PED)^{E}_{ij,h}$ and the change in the internal coordinates due to the elastic stress were also calculated by the method of Yamamoto *et al.* (1974a). The short-range parameters based on a short-range (SR) model were refined by the least-squares fit both to the observed optical mode frequencies and to the elastic constants (Yamamoto *et al.*, 1974b).

The method of a polarizable-ion (PI) model calculation of optically-active vibration frequencies of ionic crystals was described by Yamamoto *et al.* (1976). Those aspects of the PI model relevant to the present work are given below. From Born and Huang (1954, chapter 5), a dynamical matrix **D** is constructed by four constituents in the form

$$\mathbf{D} = \overline{\mathbf{M}}(\mathbf{F}^{N} + \mathbf{F}^{C} + \mathbf{F}^{I} + \mathbf{F}^{M})\overline{\mathbf{M}}$$

where $\overline{\mathbf{M}}$ denotes the inverse-mass matrix. The first term arises from short-range non-Coulomb interactions. The second is the Coulomb interaction part due to the undeformable ion interactions. The third is the Coulomb interaction part resulting from the induced dipole interactions through an electronic polarizability. The last term refers to the macroscopic field and is dependent on the direction of the propagation, whereas the first three terms are independent of the direction of the wave propagation in the long-wavelength limit.

The modified Urey-Bradley force field (Shima-

Table 3. Experimental and theoretical elastic constants (10^{11}dyn/cm^2) of forsterite

	C_{11}	C_{22}	C_{33}	C_{44}	C_{55}	C_{66}	C_{12}	C_{13}	C_{23}
Exp.	32.91	20.05	23.63	6.72	8.14	8.11	6.63	6.84	7.28
Theor.	27.34	21.57	20.72	7.16	7.45	7.44	9.18	7.84	8.61

Table 4. Dynamical parameters* for least-squares fits of various models

FC	Pair	Distance (A)	SR1	RI3[b]	PI3[b,c]
K	Si O	1.6248-1.6453	3.468	3.948	3.731
k	Mg O	2.0586-2.2170	0.456	0.502	0.502
F_1	O O	2.5563-2.5857	1.090	0.765	0.918
F_2	O O	2.7431-2.7570	0.654	0.667	0.658
f_1	O O	2.8564-2.8571 (q_1)	0.231	0.270	0.218
f_2	O O	2.9375-3.0321 (q_2)	0.193	0.166	0.203
f_3	O O	3.1246-3.1937 (q_3)	0.166	0.065	0.146
f_4	O O	3.3553-3.4083 (q_4)	0.084	0.051	0.111
f_5	Mg Si	2.7036-2.7998 (q_5)	0.151	0.037	0.195
κ			0.214	0.169	0.255
p			-0.289	-0.288	-0.274
Z_{Mg}				0.93	0.50
Z_{Si}				0.70	0.38
Z_{O}				-0.64	-0.34
χ(%)[d]			4.95	3.80	4.67

a) Units of force constant are mdyn/A, except κ of mdyn·A. Effective charge Z is in electron unit.

b) Charge distribution parameter x is 3/4.

c) Electronic polarizability and high-frequency dielectric constant are as follows:

α(Mg)=0.10, α(Si)=0.02, $\alpha_{xx}(0)$=1.55, $\alpha_{yy}(0)$=1.50, $\alpha_{zz}(0)$=1.53A^3; $\varepsilon_\infty(xx)$=2.79, $\varepsilon_\infty(yy)$=2.68, $\varepsilon_\infty(zz)$=2.73.

d) Standard deviation.

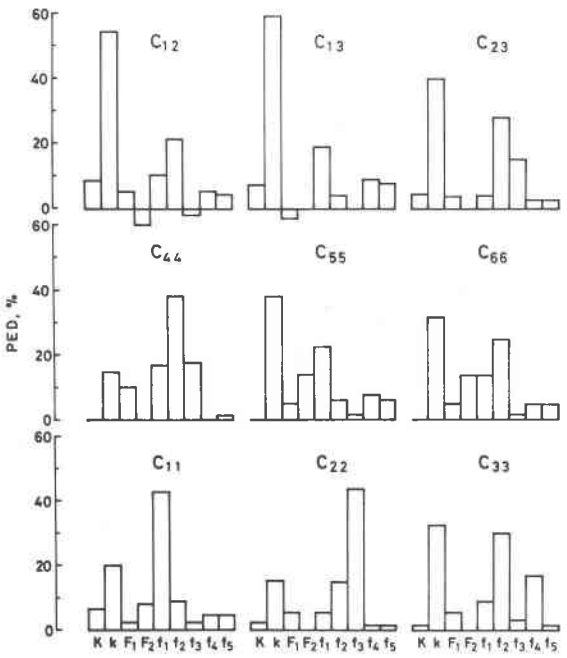

Fig. 3. Contribution (percent) of potential terms to the theoretical elastic constants of forsterite.

nouchi, 1963), which is used in the calculation of the non-Coulomb interaction part $\mathbf{F}^N$, contains the Si–O stretching force K, the non-bonded O···O repulsive forces F_1 and F_2, and the two correction terms κ of intramolecular tension and p of bond interaction for SiO_4^{4-} internal modes; it contains also the Mg–O stretching force k, the non-bonded O···O repulsive forces f_1, f_2, f_3 and f_4, and the Mg–Si interaction force f_5 for external modes.

Theoretical results and discussion

SR model and elastic constants

Theoretical optical frequencies and elastic constants are compared with the experimental data in Tables 1, 2, and 3. The calculated values of model parameters are listed in Table 4. These tables show that the set of force constants based on the SR1 model reproduces satisfactorily both the optical frequencies and the macroscopic elastic constants. Figure 3 shows the contributions of all the potential terms to the theoretical elastic constants. The potential energy contributions of the repulsive force constant F_1 to C_{12} and C_{13} are negative. Note that the potential energy of forsterite elastic constants contributes predominantly to the Mg–O stretching force and non-bonded O···O repulsive forces between SiO_4 tetrahedra. Graham and Barsch (1969) suggested that the elastic properties of forsterite are predominantly determined by the oxygen anion framework, and therefore the elastic properties of an oxide with comparatively small cations are quite independent of the nature of the cation. The present result, however, shows that the Mg–O stretching force also plays an important role in the elastic properties of forsterite, especially in C_{55}, C_{12},C_{13}, and C_{23}.

Both forsterite and corundum form a distorted hexagonal close-packed structure of the framework of oxygen ions. It is, therefore, of interest to investigate the extent to which the elastic properties of corundum are influenced by the Al–O stretching forces. Iishi (1978a) pointed out an important effect of the Al–O stretching force to the elastic property of corundum. Iishi (1978b) also pointed out that the elastic properties of quartz depend on the nature of cations occurring within anion interstices. The abnormal elastic behaviour near the α–β phase transition point of quartz is attributable both to the large negative energy contribution of torsional force to the elastic properties near the transition point, and to the large energy contribution of the Si–O stretching force to the elastic properties of β-quartz. In the forsterite–spinel phase transition the cation–anion interactions may therefore become increasingly significant, especially near the transition point.

Table 5 suggests that the change in the Mg–O stretching coordinates is sensitive to the applied stress S_{xx}, S_{yy}, and S_{zz}. On the other hand, non-bonded oxygen–oxygen repulsive coordinates q_2 and q_4 between SiO_4 tetrahedra are sensitive to the applied stress S_{yz} and S_{zx}, and S_{xy}, respectively.

Table 5. Change (A^3/mdyn) of internal coordinates due to elastic stress in forsterite

Coordinate	S_{xx} A_{1g}	S_{yy} A_{1g}	S_{zz} A_{1g}	S_{yz} B_{3g}	S_{zx} B_{2g}	S_{xy} B_{1g}
SiO str.	8.2	6.8	4.4	-1.8	0.4	-0.8
MgO str.	67.6	85.5	84.7	8.3	17.1	27.9
OSiO def.*	-0.7	-0.7	2.8	10.6	-18.3	10.6
q_1	27.0	-10.7	-21.6	-28.1	-16.9	-8.5
q_2	-9.6	-3.9	8.7	-59.6	-64.9	-7.3
q_3	-23.1	43.7	-5.2	3.4	-14.6	-22.0
q_4	-0.4	-10.8	30.2	10.6	22.3	46.9
q_5	29.5	17.5	20.2	17.7	39.1	-3.6

* *Unit of angle coordinate is Rad·A^2/mdyn.*

Table 6. Force constants, effective charges, and distribution parameter of forsterite based on RI model

FC*	RI1 x=2	RI2 x=1	RI3 x=3/4	RI4 x=1/2	RI5 x=1/5	RI6 x=-1/5	RI7 x=-1/2	RI8 x=-1	RI9 x=-2
K	4.175	4.134	3.948	3.704	3.451	3.206	3.134	3.204	3.560
k	0.495	0.511	0.502	0.504	0.507	0.488	0.441	0.389	0.473
F_1	0.554	0.775	0.765	0.856	0.945	1.014	1.012	0.868	0.993
F_2	0.719	0.592	0.667	0.702	0.736	0.767	0.807	0.834	0.578
f_1	0.125	0.228	0.270	0.296	0.319	0.358	0.371	0.361	0.227
f_2	0.129	0.149	0.166	0.175	0.186	0.204	0.221	0.251	0.206
f_3	0.123	0.068	0.065	0.068	0.074	0.086	0.098	0.124	0.138
f_4	0.084	0.051	0.051	0.051	0.052	0.054	0.056	0.061	0.094
f_5	0.143	0.023	0.037	0.035	0.036	0.085	0.175	0.258	0.167
κ	0.430	0.185	0.169	0.181	0.199	0.205	0.231	0.339	0.284
p	-0.150	-0.230	-0.288	-0.332	-0.369	-0.390	-0.384	-0.312	-0.219
Z_{Mg}	0.51	0.86	0.93	0.95	0.96	0.96	0.89	0.80	0.36
Z_{Si}	1.02	0.86	0.70	0.48	0.19	-0.19	-0.45	-0.80	-0.72
Z_O	-0.51	-0.65	-0.64	-0.59	-0.53	-0.43	-0.33	-0.20	0.00
χ(%)	3.98	3.97	3.80	3.81	3.99	4.26	4.31	4.31	4.96

* *Notations and units are the same as in Table 4.*

RI model

It must be remembered that, because forsterite contains SiO_4^{4-} tetrahedra, the distribution of the effective charge on the group cannot be known beforehand. The magnitude of the effective charge of a Mg ion is set to be Z and the distribution of effective charge of a Si and an O is set to be xZ and $-(x + 2)Z/4$, respectively. Several trial sets of charge distribution were assumed under electrostatically neutral condition in the whole crystal. With various values of parameter x, both the magnitude of Z and the values of short-range force constant were fitted to the experimental phonon frequencies, both ν_{TO} and ν_{LO}. The relation between short-range force constants and effective charges at several values of the distribution parameter are listed in Table 6. The magnitude of a *TO–LO* splitting which is sensitive to the distribution parameter is shown in Figure 4.

Figure 4 shows that when the charge distribution parameter x is negative (*i.e.* if the charge of a Si ion is negative), the magnitudes of theoretical *TO–LO* splitting are very small compared with the experimental results, especially in the high-frequency region. When the charge distribution parameter x is 2 (*i.e.* if the ionic character of a Mg ion and a Si ion is the same), the magnitudes of a theoretical *TO–LO* splitting are small compared with those of the experimental one. When a charge distribution parameter x is between x = 1 and x = 1/5, some short-range force constants change gradually but the magnitude of an effective charge Z is seen to fall into the range between 0.86 and 0.96e. The charge distribution model of x = 3/4 gives the best result. With this charge distribution, the effective charges of Mg, Si, and O ions are as follows; $Z_{Mg} = 0.93$, $Z_{Si} = 0.70$ and $Z_O = -0.64e$. The best-fit calculated frequency of the RI3 model is listed in Tables 1 and 2.

As a typical example, the theoretical vibrational modes of B_{2u} based on the RI3 model are shown in Figure 5. There is little or no displacement of Mg^{2+} ion in the internal stretching modes ν_3 and ν_1 at the high-frequency region. There is a small displacement of Mg^{2+} ion in the internal bending mode ν_4, though it cannot be shown by arrows, and a fairly large displacement in the ν_2 at the medium-frequency region.

All the external frequencies in the low-frequency region are more or less mixing modes of the rotation

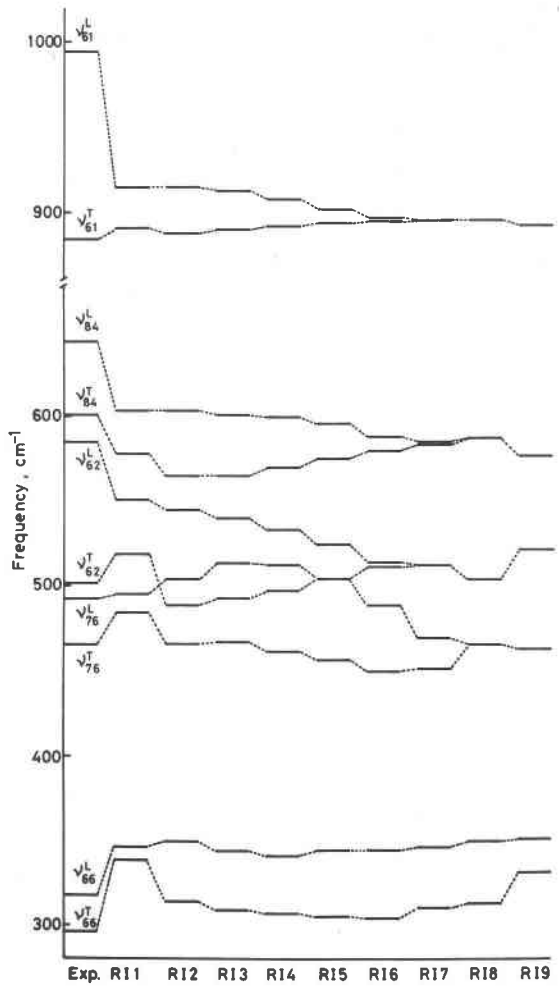

Fig. 4. *TO–LO* splittings of experimental measurement and theoretical model.

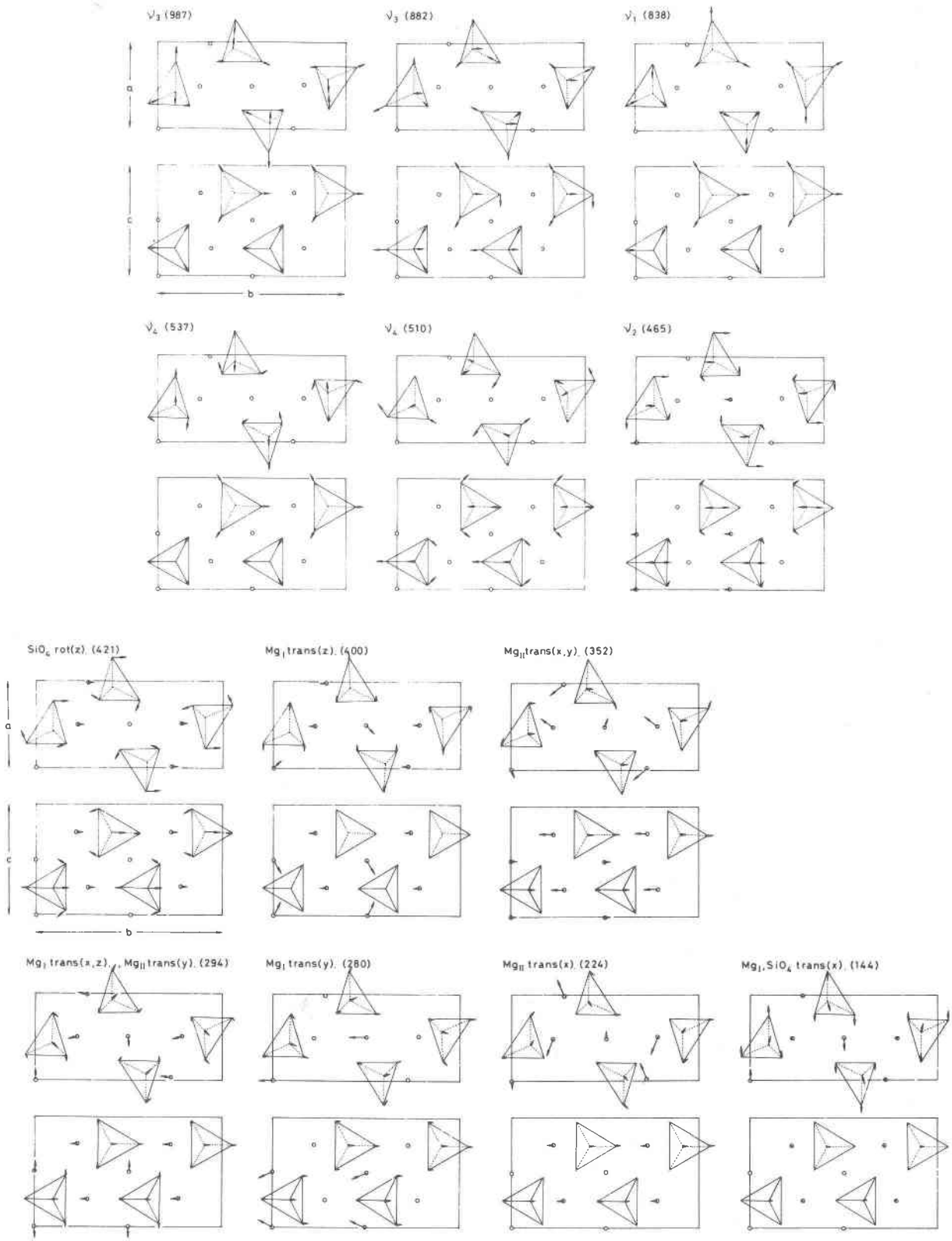

Fig. 5. Theoretical vibrational modes of $B_{2u}(TO)$ symmetry based on the R13 model.

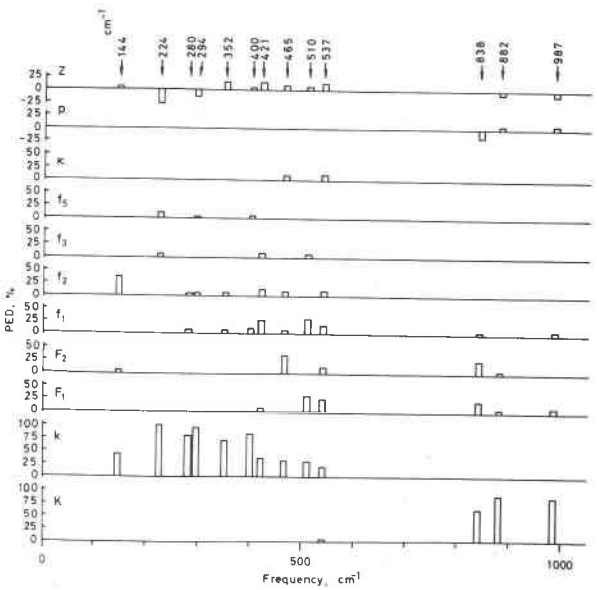

Fig. 6. Contribution (percent) of potential terms to potential energy in normal frequencies of $B_{2u}(TO)$ symmetry.

of SiO_4^{4-} ion and the translation of SiO_4^{4-} ion and/or Mg^{2+} ion. These external modes are probably assignable as follows: the phonon frequency at 421cm^{-1} is the rotational mode of SiO_4^{4-} along the z axis; frequencies at 400 and 280cm^{-1} are the translational modes of Mg^{2+} ion at MgI site along the z axis and x axis, respectively; frequencies at 352 and 224cm^{-1} are the translational mode of Mg^{2+} ion at MgII site along the y and x axes and the x axis, respectively; the frequency at 294cm^{-1} is the mixing mode of a translational mode of Mg^{2+} ion at MgI site and that at MgII site; and the lowest phonon frequency at 144cm^{-1} is the mixing translational mode of both Mg^{2+} ion at MgI site and SiO_4^{4-} ion along the x axis.

As is stated above, all frequency modes are assigned acccording to theoretical vibrational modes and the results are shown in Tables 1 and 2. The present assignment, deduced theoretically, agrees well with the assignment experimentally determined by Tarte (1963), Paques-Ledent and Tarte (1973, 1974), and Paques-Ledent (1976) according to the systematic investigation of infrared and Raman spectra of olivine-type compounds.

Ochler and Günthard (1969) proposed a detailed interpretation of the infrared spectrum of forsterite on the basis of a normal coordinate treatment, followed by the computation of the fundamental frequencies deduced from a convenient set of force constants. As was pointed out by Paques-Ledent and Tarte (1973), the assignment proposed by Ochler and Günthard was rejected; the frequency shifts obtained from isotropic data could not be interpreted by their assignment. The present assignment, however, agrees well with experimental data. There appears to be a complete, unambiguous correlation between the experimental frequencies and the various vibrational modes derived theoretically.

The contribution (percent) of potential terms to potential energy (PED) in each normal frequency of $B_{2u}(TO)$ symmetry is shown in Figure 6 as a typical example. It shows clearly that the contributions of potential terms to potential energy in the internal stretching modes, the internal bending modes, and the external modes are very different from each other.

In Figure 7 the dependence of phonon frequencies of $B_{2u}(TO)$ and A_g symmetry on the effective ionic charge is shown as a typical example. The behaviour of the translational lattice vibrations of the 224cm^{-1} mode of B_{2u}(TO) and the 183cm^{-1} mode of A_g is typical of the instability of forsterite crystal caused by dynamical phenomena. It appears that critical hardening of the internal bending modes and the rotational modes of SiO_4^{4-} ion may be displayed at the approach of the instability of the crystal.

The obtained interatomic constants of non-bonded oxygen–oxygen interaction are plotted as a function of interatomic distances in Figure 8. The Lennard-Jones potential constants, A and B, of the form (Fowler, 1936, p. 292–337):

$$U(r) = -A/r^6 + B/r^9,$$

can be determined by the use of the relation:

$$f(r_0) = [d^2U/dr^2]_{r = r_0},$$

where $f(r_0)$ is the force constant at the interatomic distance of r_0. In this figure, the curve is drawn using the values $A = 600 \times 10^{-6}$ erg·cm^6 and $B = 87.8 \times 10^{-82}$ erg·cm^9. The force constants of large inter-

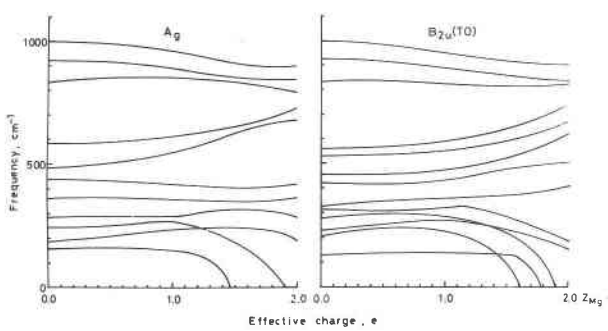

Fig. 7. Dependence of phonon frequencies of $B_{2u}(TO)$ and A_g symmetries on effective ionic charges.

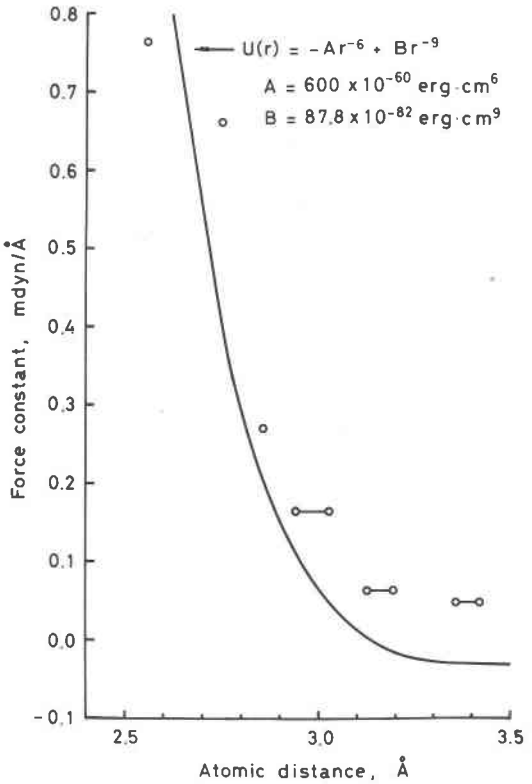

Fig. 8. Force constants for non-bonded oxygen-oxygen interactions of forsterite. Lennard-Jones potential $U(r) = -A/r^6 + B/r^9$ is drawn by use of the constants $A = 600 \times 10^{-60}$ erg·cm^6 and $B = 87.8 \times 10^{-82}$erg·cm^9.

atomic distance are somewhat larger than the values expected from the Lennard-Jones type potential.

PI model

The electric polarizabilities of the magnesium ion and the silicon ion were fixed at 0.10 and 0.02A^3, respectively, according to Tessman *et al.* (1953). The electronic polarizability of the oxygen ion was determined to reproduce the refractive indices, $\alpha = 1.636$, $\beta = 1.651$, and $\gamma = 1.669$. From the RI model result, the charge distribution parameter x was fixed at x = 3/4. The best-fit dynamical value of dynamical parameters and the theoretical frequency are listed in Table 4 and Tables 1 and 2, respectively. In spite of the more elaborate nature of the present PI model, the agreement for the optical frequency was worse compared with the RI model. The result was not improved by considering both another set of ionic charge distributions and another set of electronic polarizabilities of the magnesium, silicon, and oxygen ions. As was demonstrated by Iishi (1978a), the short-range interactions of electronic and atomic displacement should be considered in order to reproduce the magnitudes of the *TO–LO* splitting of all frequency modes. A treatment based on a well-known shell model (Cochran, 1971) may be the best approach at present.

Acknowledgments

The author thanks Professor Dr. E. Eberhard for financial support and for the use of the computer in the regional Rechen-Zentrum für Niedersachsen in Hannover, and the Alexander von Humboldt-Foundation for a fellowship. The crystal of forsterite was grown by Dr. H. Takei. The author is grateful for the use of the crystal. He is also greatly indebted to Dr. E. Salje and Mr. G. Hoppman for their assistance in measuring the infrared reflection and Raman spectra.

References

Birle, J. D., G. V. Gibbs, P. B. Moore and J. V. Smith (1968) Crystal structures of natural olivines. *Am. Mineral., 53,* 807–824.

Born, M. and K. Huang (1954) *Dynamical Theory of Crystal Lattices.* Oxford University Press, London.

Chen, S. H. (1967) Group-theoretical analysis of lattice vibrations in metallic β-Sn. *Phys. Rev., 163,* 532–546.

Cochran, W. (1971) Lattice dynamics of ionic and covalent crystals. *CRC Critical Reviews in Solid State Sciences, 2,* 1–44.

Duke, D. A. and J. D. Stephens (1964) Infrared investigation of the olivine group minerals. *Am. Mineral., 49,* 1388–1406.

Fowler, R. H. (1936) *Statistical Mechanics.* Cambridge University Press, London.

Graham, E. K. and G. R. Barsch (1969) Elastic constants of single-crystal forsterite as a function of temperature and pressure. *J. Geophys. Res., 74,* 5949–5959.

Iishi, K. (1978a) Lattice dynamics of corundum. *Phys. Chem. Minerals, 3,* 1–10.

——— (1978b) Lattice dynamical study of the α–β quartz phase transition. *Am. Mineral., 63,* 1190–1197.

Ochler, O. and Hs. H. Günthard (1969) Low-temperature infrared spectra between 1200 and 20 cm^{-1} and normal-coordinate analysis of silicates with olivine structure. *J. Chem. Phys., 51,* 4719–4728.

Paques-Ledent, M. Thn. (1976) Vibrational studies of olivine-type compounds—III. Orthosilicates and germanates $A^IB^{III}X^{IV}O_4$. *Spectrochim. Acta, 32A,* 383–395.

——— and P. Tarte (1973) Vibrational studies of olivine-type compounds—I. The i.r. and Raman spectra of the isotropic species of Mg_2SiO_4. *Spectrochim. Acta, 29A,* 1007–1016.

——— and——— (1974) Vibrational studies of olivine-type compounds—II. Orthophosphates, -arsenates and -vanadates $A^IB^{II}X^VO_4$. *Spectrochim. Acta, 30A,* 673–689.

Salje, E. (1974) Ramanspektroskopische Untersuchungen an KJO_3-Kristallen. *Z. Kristallogr., 139,* 317–334.

——— and K. Iishi (1977) Ferroelastic phase transitions in lead phosphate-vanadate $Pb_3(P_xV_{1-x}O_4)_2$. *Acta Crystallogr., A33,* 399–408.

Servoin, J. L. and B. Piriou (1973) Infrared reflectivity and Raman scattering of Mg_2SiO_4 single crystal. *Phys. stat. sol. (b), 55,* 677–686.

Shimanouchi, T. (1963) Force constants of small molecules. *Pure Appl. Chem., 7,* 131–145.

Shiro, Y. and T. Miyazawa (1971) A general matrix method for

treating elastic constants of molecular crystals: application to orthorhombic polyethylene. *Bull. Chem. Soc. Japan, 44,* 2371–2373.

Takei, H. and T. Kobayashi (1974) Growth and properties of Mg_2SiO_4 single crystals. *J. Cryst. Growth, 23,* 121–124.

Tarte, P. (1963) Etude infra-rouge des orthosilicates et de orthogermanates—II. Structures du type olivine et monticellite. *Spectrochim. Acta, 19,* 25–47.

Tessman, J. R., A. H. Khan and W. Shockley (1953) Electronic polarizabilities of ions in crystals. *Phys. Rev., 92,* 890–895.

Yamamoto, A., Y. Shiro and H. Murata (1974a) Optically-active vibrations and elastic constants of calcite and aragonite. *Bull. Chem. Soc. Japan, 47,* 265–273.

———, ——— and ——— (1974b) The optically-active vibration and elastic constant of soda-niter. *Bull. Chem. Soc. Japan, 47,* 1105–1112.

———, T. Utida, H. Murata and Y. Shiro (1976) Coulomb interactions and optically-active vibrations of ionic crystals—I. Theory and application to $NaNO_3$. *J. Phys. Chem. Solids, 37,* 693–698.

Manuscript received, December 12, 1977; accepted for publication, March 30, 1978.